REPORT DOCUMENTATION PAGE

Form Approved
OMB No. 0704-0188

PLEASE DO NOT RETURN YOUR FORM TO THE ABOVE ORGANIZATION.

1. REPORT DATE *(DD-MM-YYYY)*	2. REPORT TYPE	3. DATES COVERED *(From - To)*
31-03-2010	Final Technical Report	1 July 2006 - 31 December 2009

4. TITLE AND SUBTITLE
(AFRL NANOTECHNOLOGY INITIATIVE) HYBRID NANOMATERIALS IN PHOTONIC CRYSTAL CAVITIES FOR MULTI-SPECTRAL INFRARED DETECTOR ARRAYS

5a. CONTRACT NUMBER

5b. GRANT NUMBER
FA9550-06-1-0482

5c. PROGRAM ELEMENT NUMBER

6. AUTHOR(S)
Stiff-Roberts, Adrienne D. (PI)
Zhou, Weidong (co-PI)

5d. PROJECT NUMBER

5e. TASK NUMBER

5f. WORK UNIT NUMBER

7. PERFORMING ORGANIZATION NAME(S) AND ADDRESS(ES)
Duke University
Office of Research Support
2200 West Main Street, Ste 710
Durham, NC 27705-4677

The University of Texas at Arlington
Office of Grant and Contract Services
202 East Border Street, Ste 216
Arlington, TX 76019-0145

8. PERFORMING ORGANIZATION REPORT NUMBER
313-6060-602430000

9. SPONSORING/MONITORING AGENCY NAME(S) AND ADDRESS(ES)
Duke University
Office of Sponsored Programs
Box 104135
Durham, NC 27708

10. SPONSOR/MONITOR'S ACRONYM(S)

11. SPONSOR/MONITOR'S REPORT NUMBER(S)

12. DISTRIBUTION/AVAILABILITY STATEMENT
Approved for public release.

13. SUPPLEMENTARY NOTES

14. ABSTRACT
The goal of this project was to demonstrate the feasibility of a multi-spectral infrared (IR) photodetector using hybrid nanomaterials in photonic crystal (PC) cavities for enhanced absorption at selected wavelengths. The simultaneous sensing of multiple IR wavelengths, particularly in the near-IR and mid-IR, is important because it enables intelligent surveillance, target recognition, and chem-bio detection. This project investigated InAs/GaAs epitaxial quantum dots (EQDs) and colloidal quantum dots (CQDs). By incorporating these nanomaterials in one-dimensional (1D) and two-dimensional (2D) PC cavities, the possibility of multi-spectral configurability and enhanced absorption was explored. It was demonstrated that integrating EQDs with 2D PC cavities (etched air holes) is challenging due to difficulty in matching photonic bandgap defect modes with InAs/GaAs EQD absorption peaks. Nonetheless, enhanced absorption was demonstrated in a specific defect mode at 8 um at low temperatures. In contrast, it was straightforward to enhance absorption at specific wavelengths at room temperature by integrating CQDs with 1D PC cavities (polymer distributed Bragg reflectors). An enabling technology was matrix-assisted pulsed laser evaporation.

15. SUBJECT TERMS
infrared photodetection, quantum dots, photonic crystal cavities, matrix-assisted pulsed laser evaporation

16. SECURITY CLASSIFICATION OF:			17. LIMITATION OF ABSTRACT	18. NUMBER OF PAGES	19a. NAME OF RESPONSIBLE PERSON
a. REPORT	b. ABSTRACT	c. THIS PAGE			Adrienne D. Stiff-Roberts
U	U	U	UU	16	19b. TELEPHONE NUMBER *(Include area code)* 919-660-5560

Reset

Executive Summary

The overall goal of this project was to demonstrate the feasibility of a multi-spectral infrared (IR) photodetector using hybrid nanomaterials in photonic crystal (PC) cavities for enhanced absorption at selected wavelengths. The simultaneous sensing of multiple IR wavelengths, particularly in the near-IR (1-3 μm) and mid-IR (3-5 μm) ranges, is important because it enables intelligent surveillance, target recognition, and chem-bio detection. Typically, multi-spectral IR photodetection is realized by device heterostructures comprising active regions with varying material composition, such as bulk $Hg_xCd_{1-x}Te$ photodiodes. The ability of this approach to realize a wide range of spectral sensitivity is inherently limited by the epitaxial growth system. An alternative approach investigated by this program is the integration of hybrid nanomaterial active regions in a single device heterostructure. More specifically, this project investigated InAs/GaAs epitaxial quantum dots (EQDs) grown by strained-layer epitaxy and colloidal quantum dots (CQDs) synthesized by inorganic chemical reactions. By incorporating these nanomaterials in one-dimensional (1D) and two-dimensional (2D) PC cavities, the possibility of multi-spectral configurability and enhanced absorption was explored.

As a result of the work conducted in this project, it was demonstrated that integrating EQDs with 2D PC cavities (specifically etched air holes) is very challenging due to the difficulty in matching photonic bandgap defect modes with InAs/GaAs EQD absorption peaks. While enhanced absorption was demonstrated in a specific defect mode at 8 μm, this effect was observed at very low temperatures (17K). In contrast, it is very straightforward to enhance absorption and to provide spectral selectivity at room temperature by integrating CQDs with 1D PC cavities (specifically organic polymer distributed Bragg reflectors). An important enabling technology that provided this result was matrix-assisted pulsed laser evaporation for the deposition of organic-based materials. Another important result of this project is that a new type of device that integrates CQDs with 2D PC cavities was demonstrated, the Fano resonance filter, which also provides room temperature absorption enhancement in a straightforward manner.

Research Accomplishments

The investigation of the feasibility of hybrid nanomaterial, multi-spectral, photonic crystal infrared photodetectors has yielded significant research accomplishments towards the ultimate goal of demonstrating enhanced absorption and spectral selectivity. In addition, many other important results were achieved:

- Demonstrated that it is worthwhile to further investigate the use of Sb-based materials in IR photodetectors, namely InSb/GaAs EQDs to achieve far-IR (> 14 μm) photodetection and GaSb-based PCs for application to Sb-based strained-layer superlattices.
- Identified an important charge leakage mechanism in InAs/GaAs EQDs grown by molecular beam epitaxy (MBE) due to silicon doping in GaAs that results in higher dark current densities and reduced quantum dot activation energies. Also demonstrated the novel use of cross-sectional scanning capacitance microscopy (SCM) to investigate dopant incorporation in InAs/GaAs EQDs.
- Demonstrated room-temperature, mid-IR photodetection in hybrid nanocomposite quantum dot infrared photodetectors (QDIPs) based on intraband transitions in CdSe CQDs.
- Developed novel emulsion-based target for organic thin-film deposition by matrix-assisted pulsed laser evaporation (MAPLE) that yielded polymer films with state-of-the-art structural characteristics applicable to optoelectronic devices.

- Demonstrated enhanced absorption and spectral selectivity of EQDs and CQDs at specific IR wavelengths by incorporating these nanomaterials in PC cavities (either 1D or 2D).
- Demonstrated a new type of spectrally selective photodetector with enhanced absorption based on Fano resonance filters in PCs with tunable optical properties based on filling fabricated air-holes in nanomembranes with CQDs by MAPLE.

Feasibility of Sb-Based Epitaxial Quantum Dots for Far-Infrared Photodetection and Sb-based Photonic Crystals for Strained-Layer Superlattices

Sb-based materials could be an important technology for IR photodetection because: i) InSb/GaAs EQDs could extend the spectral response of QDIPs to include far-IR wavelengths; and ii) GaSb-based PCs are also applicable to strained-layer superlattice devices and could provide enhanced absorption in these IR photodetectors. This project determined the feasibility of using Sb-based materials in infrared photodetectors, both as the EQD active region and the PC cavity.

An interesting aspect of the InSb/GaAs heterojunction is that it has a lattice mismatch of 14.6%, indicating that quantum dot formation should occur in the Volmer-Weber growth mode. As a result, the two-dimensional wetting layer present in the Stranski-Krastanow growth mode typical of InAs/GaAs EQDs should be absent. Volmer-Weber EQDs could significantly impact QDIP performance because the wetting layer often reduces carrier confinement in the EQD. The studies of InSb/GaAs QD growth focused on demonstrating Volmer-Weber growth on (001) GaAs substrates. Variations in substrate temperature and III:V flux ratio were investigated. The best results from these studies are shown in the planar atomic force microscopy (AFM) and cross-sectional transmission electron microscopy (XTEM) images of Figs. 1(a) and (b), respectively. These images correspond to 3 ML InSb/GaAs QDs grown at 375 °C with a III:V flux ratio of 1:2. From the AFM image, the EQD surface density is $3.06\times10^{10}/cm^2$ and the average EQD diameter is 39.6 nm. Importantly, the EQD surface density is almost an order of

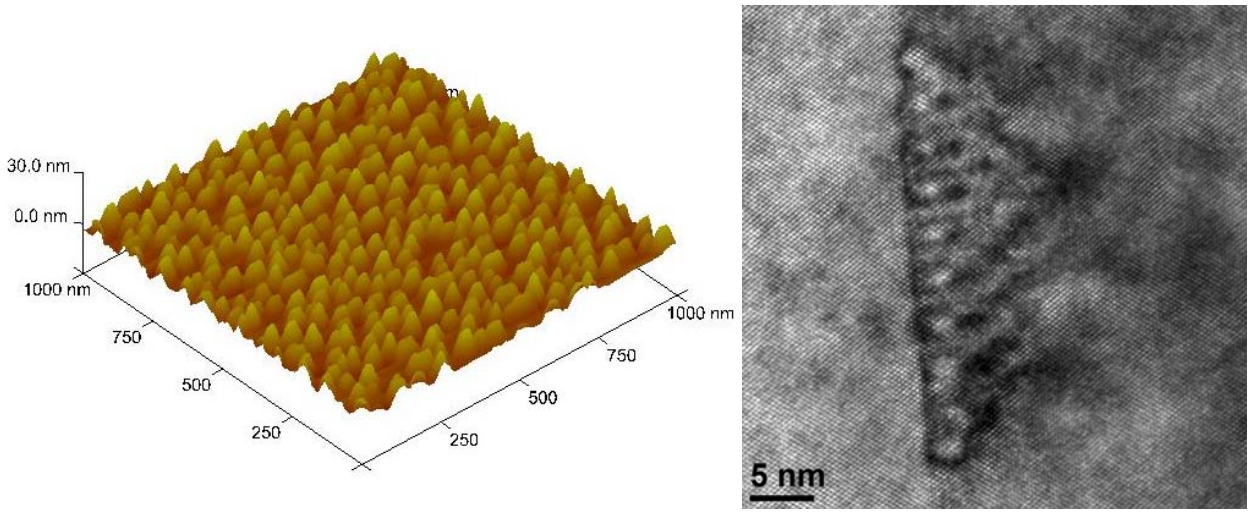

(a) (b)

Figure 1. (a) Planar AFM and (b) high-resolution XTEM images of InSb/GaAs EQDs grown in the V-W growth mode by MBE at Duke.

magnitude higher than most reports in literature, which is significant for application as the absorption region in QDIPs. The XTEM image clearly demonstrates that a pyramidal InSb QD is buried in the GaAs matrix. This image also seems to indicate that a 2D wetting layer is not present in these dots, as expected for V-W growth. However, further studies are required to clearly demonstrate that no wetting layer is present. A significant challenge to using these EQDs in device heterostructures is the build-up of strain that could negatively impact the growth of multiple dot layers required for efficient IR absorption due to threading dislocations. Nonetheless, the results obtained in this project demonstrate that while Sb-based materials are challenging, it is worthwhile to investigate these materials further for application to IR photodetection.

The fabrication of GaSb-based PC cavities required the development of processes for the patterning and dry-etching of GaSb PC cavities in order to obtain smooth and straight side-walls of the etched air holes. The etching quality achieved in these GaSb PCs is comparable to that of fabricated GaAs PCs. These results are shown in the scanning electron microscopy (SEM) images of Fig. 2. The etching results in this work can be further improved with process optimization, but demonstrate that GaSb-based PC cavities of high quality can be achieved, which is an important demonstration that could aide in improving the performance of Sb-based strained layer superlattice IR photodetectors.

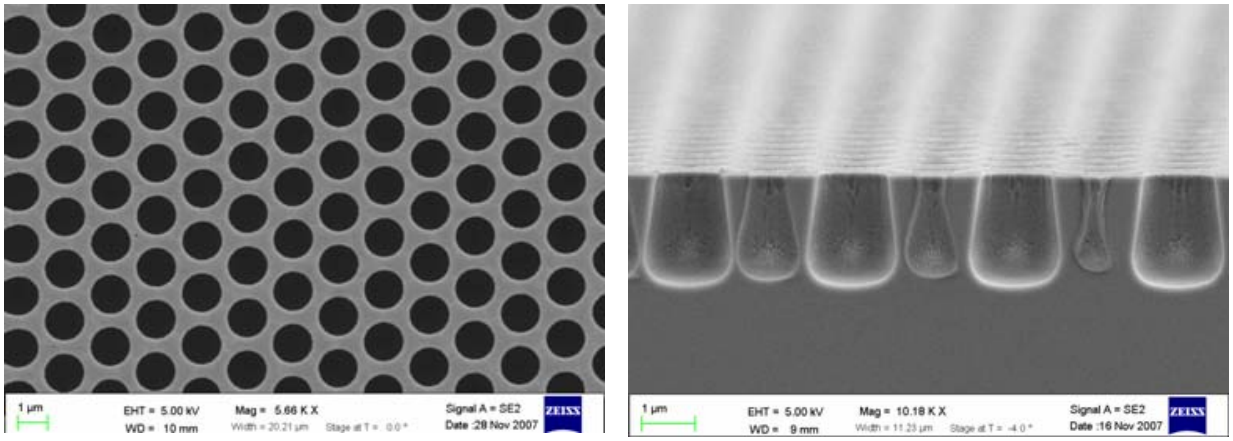

(a) (b)

Figure 2. (a) Top- and (b) side-view SEM images of GaSb PCs fabricated at UT-Arlington.

Understanding Dopant Incorporation in InAs/GaAs Epitaxial Quantum Dots Grown by Molecular Beam Epitaxy

By exerting better control over dopant incorporation during MBE growth, it should be possible to improve IR photodetector performance by reducing dark current (leading to higher operating temperatures and enhanced detectivity) and selectively occupying confined energy levels (leading to more controlled tuning of the IR spectral response). Using polarization-dependent, Fourier transform infrared (FTIR) absorbance spectroscopy to investigate InAs/GaAs QDIP heterostructures featuring different remote doping schemes, this work observed a peak at 405 meV, an energy that is greater than the range of EQD intraband transitions, and demonstrates signature characteristics of donor-complex defect levels (or DX centers) in III-V semiconductors (Si-doped GaAs). These characteristics include spherical symmetry, thermal activation of trapped carriers with increasing temperature, and dependence of absorbance peak

magnitude (and thereby DX center concentration) on doping concentration and doping scheme. While DX centers are known to exist in these materials, their influence on the performance of QDIPs has not been elucidated previously.

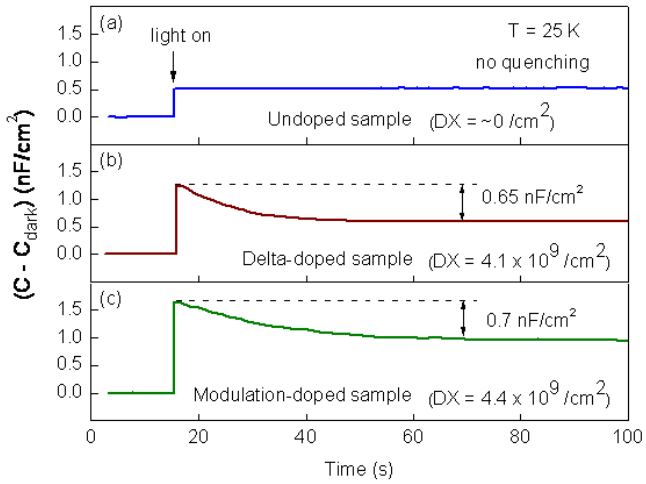

Figure 3. Transient photocapacitance per unit area for (a) undoped, (b) delta-doped, and (c) modulation-doped EQD Schottky diodes at 25 K demonstrating quenching in doped devices only. Estimated DX center concentrations are indicated in parentheses.

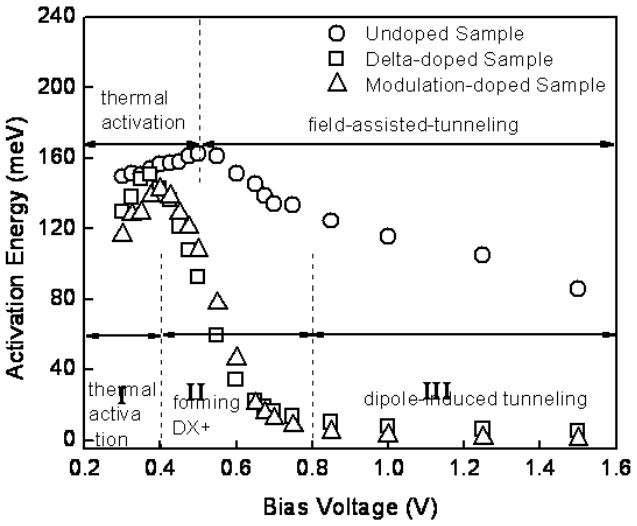

Figure 4. EQD activation energy as a function of bias voltage determined from dark current Arrhenius plots for undoped (circle), delta-doped (square), and modulation-doped (triangle) EQD Schottky diodes, demonstrating different, bias-dependent transport mechanisms for undoped and doped devices.

For further verification of the existence of DX centers in Si-doped InAs/GaAs EQDs, three, EQD Schottky diodes [one undoped, one modulation-doped, and one delta-doped] were grown by solid source MBE for device characterization. Photocapacitance-time spectra were measured because the quenching of photocapacitance with time can be used to detect the existence of DX center metastable states. Fig. 3 shows the transient photocapacitance per unit device area. No appreciable photocapacitance quenching is observed for the undoped sample, while both doped samples demonstrate quenching. This measurement provides strong evidence of the existence of DX centers in Si-doped, InAs/GaAs EQDs.

Dark current-voltage spectra were measured for temperatures ranging from 35-300 K, thereby enabling the determination of bias-dependent EQD activation energies by Arrhenius plots. Fig. 4 shows the EQD activation energies as a function of bias voltage for the undoped, delta-doped, and modulation-doped EQD Schottky diodes. For the undoped sample, the EQD activation energy ranges from 160-80 meV, consistent with thermal activation and field-assisted tunneling through the triangular potential barrier provided at higher bias voltages. In contrast, three bias-dependent regions of the EQD activation energy can be identified for the doped samples, as shown in Fig. 4. In Region I (< 0.4 V), the EQD activation energies are greater than 120 meV, consistent with thermal activation from EQD confined levels to the GaAs conduction band edge. In Region II (0.4 V to 0.8 V), the EQD activation energies of the doped samples experience a rapid decrease from 140 meV to less than 15 meV. In Region III (> 0.8 V), the EQD activation energies of the doped samples saturate below 15 meV.

The following proposed mechanism could explain the above bias dependence of the activation energy. Fig. 5 shows the conduction band energy diagram of the EQD active region, as well as the Si dopant and DX center metastable state energy levels [DX center levels when zero (DX+), one (DX_o), and two (DX-) electron(s) occupy the defect]. A dipole field can form between the DX+ center and an electron confined in a nearby EQD by Coulomb interactions. This dipole field can modify the local band structure and change the electron emission energy from the EQD. As a result, the electrostatic dipole field from the DX+ centers can induce tunneling from confined energy levels in the EQD, and electrons can escape with much smaller activation energies in doped QDIPs. Therefore, this work has identified an important charge leakage mechanism in QDIPs, namely, dipole-induced tunneling due to Si-induced DX centers in GaAs. The consideration of DX centers in QDIPs is necessary to better understand detector performance since defect centers affect activation energy, dark current, and charge dynamics in QDIPs.

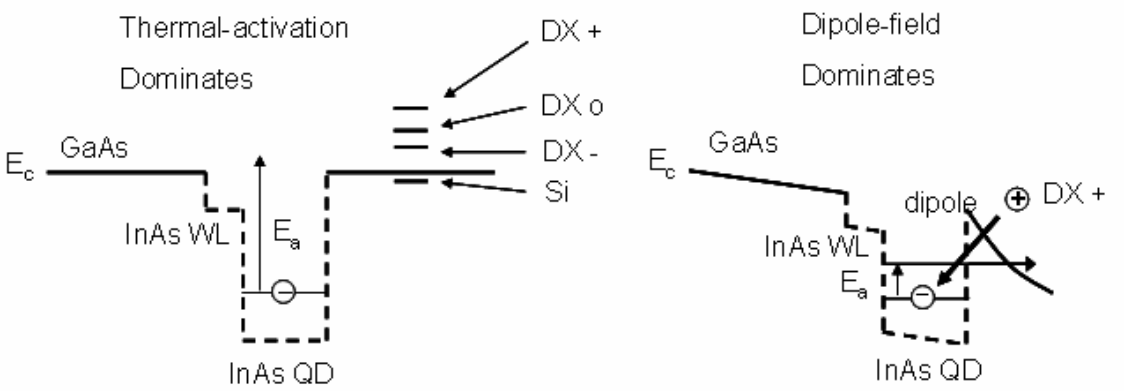

Figure 5. Conduction band energy diagrams of the EQD active region in the thermal-activation dominated and dipole-field dominated regions. Note that the DX-, DX_o, and DX+ energy levels are indicated.

This project produced another important result related to investigating dopant incorporation, that is, the novel demonstration of scanning capacitance microscopy (SCM) to determine the cross-sectional doping profile of InAs/GaAs QDIP heterostructures. This work is unique in that: i) cross-sectional SCM mapping of dopant distribution in a multi-layer EQD sample provides a microscopic, spatial representation of dopant incorporation relevant to QDIP operation, and ii) the heterostructure of the multilayer InAs/GaAs EQD sample is designed to enable a comparison between direct-doping in InAs EQD layers and remote-doping in GaAs barrier layers schemes featuring different doping concentrations. This demonstration of cross-sectional SCM to evaluate doping in an EQD heterostructure provides a new technique to better understand the relationships among doping, carrier occupation, and transport in QDIPs.

A multi-layer InAs/GaAs EQD heterostructure was designed and grown on a semi-insulating (100) GaAs substrate by solid source MBE using a Riber 2300 system. Six single EQD layers with different doping schemes and doping concentrations were grown. Each single EQD layer is separated by a 120 nm GaAs barrier layer. The bottom three dot layers were directly-doped in the InAs EQDs, while the top three dot layers were remotely-doped over 4 nm thickness in the GaAs barrier at 2 nm above the InAs EQD layer. The nominal doping concentrations for both the direct- and remote-doping EQD layers are 12, 6, and 2 electrons per dot, from bottom to top, respectively.

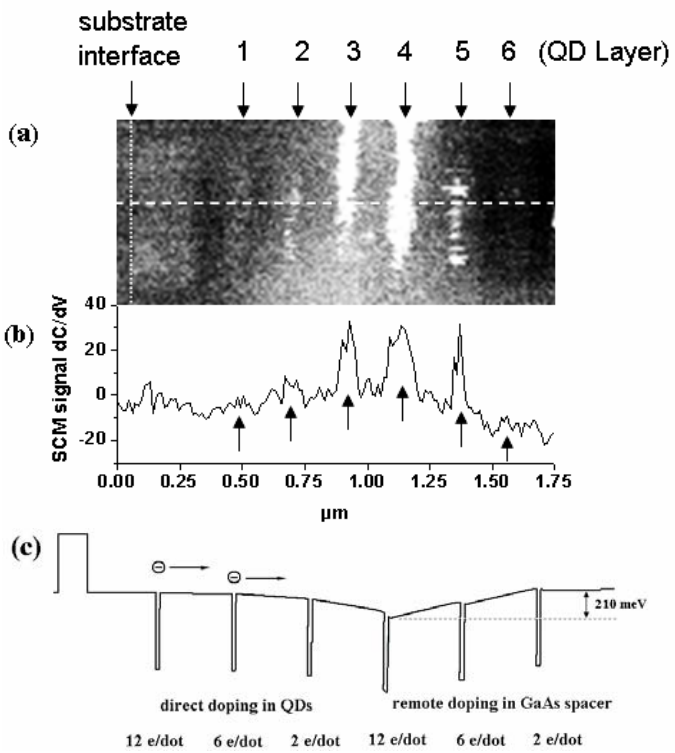

Figure 6. (a) Cross-sectional SCM image (0.8 μm x 1.75 μm) of etched EQD heterostructure; (b) SCM signal profile along the dashed line in (a); and (c) Calculated bandstructure obtained from 3D effective-mass Schrödinger–Poisson method using the Nextnano[3] semiconductor nanostructure simulation package.

A Veeco NanoScope V scanning probe microscope was used to conduct cross-sectional SCM imaging. The cross-sectional SCM measurements were carried out using native oxide on the sample surface as a thin insulator layer. Fig. 6(a) shows the SCM image (0.8 μm x 1.75 μm) and Fig. 6(b) shows the SCM signal cross-sectional profile along the dashed line in 6(a). The EQD layers have been identified by arrows. The SCM image shows the strongest signal for EQD layer four (12 electrons/dot, remote-doping), followed by layers three (2 electrons/dot, direct-doping) and five (6 electrons/dot, remote-doping). The intensity of the SCM signal should be proportional to local carrier concentration. However, the strong SCM signal appearing at EQD layer three conflicts with the low doping concentration of two electrons per dot. This contradiction suggests electron redistribution may exist in this structure. In order to verify electron redistribution in the sample, the bandstructure was calculated from the 3D effective-mass Schrödinger–Poisson method using the Nextnano[3] semiconductor nanostructure simulation package, as shown in Fig. 6(c). The simulated bandstructure shows that a large band-bending (210 meV) occurs at EQD layer four; thereby pulling down the conductive band edge of nearby EQD layers (layers three and five). As a result, the electrons in this multi-layer EQD heterostructure are relocated to the EQD layers with lower conduction band energy. This interpretation is consistent with the SCM image. The SCM image and the corresponding bandstructure calculation lead to a better understanding of doping in EQD structures, namely: i) significant band-bending can be induced by the remote-doping method, and ii) electrons provided by direct-doping in EQDs can be relocated easily due to bandstructure changes. Such easily relocated electrons may be one of the sources of dark current in QDIPs.

Room-temperature, Mid-Infrared Photodetection in Organic/Inorganic Hybrid Nanocomposite Photodetectors

To date, IR photodetectors that have been reported using CQDs embedded in conducting polymer matrices demonstrate IR photodetection in the near-IR regime (1-3 μm) corresponding to the semiconductor nanocrystal bandgap energy, as in PbS and PbSe CQDs. These devices rely on bipolar, interband (or excitonic) transitions. However, in order to reach mid- and long-wave-IR windows, extrinsic photodetection (i.e., $E_{photon} < E_{bandgap}$), such as that provided by intraband

transitions, is required. The unique approach demonstrated in this work was the use of unipolar, intraband, IR transitions in CQDs with visible bandgaps that were embedded in a conducting polymer with a large HOMO-LUMO energy gap. This project demonstrated room-temperature, mid-infrared absorption in CdSe CQD/MEH-PPV polymer nanocomposites drop-cast on GaAs substrates due to such intraband transitions. Further, by controlling the semiconductor substrate material, doping type, and doping level, the intraband, IR response can be tuned within a wide range of absorbance peaks, as observed by FTIR absorbance.

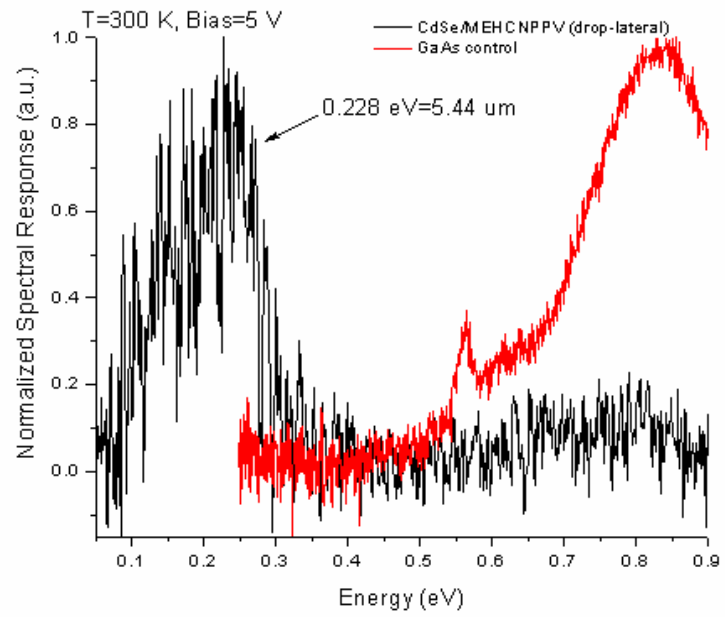

Figure 7. Room-temperature, mid-IR spectral responsivity of the photoconductor.

In addition to these FTIR absorbance measurements, this work demonstrated a room-temperature, intraband, mid-IR two-terminal photoconductor fabricated using CdSe /MEH-CN-PPV hybrid nanocomposites deposited by drop-casting on GaAs. Fig. 7 shows the room-temperature spectral responsivity of the hybrid nanocomposite IR photodetector for applied bias of 5V. This work represents an important demonstration of a fundamentally different organic/inorganic hybrid nanocomposite IR photodetector.

MAPLE Deposition of Conducting Polymer Thin Films Using an Emulsion Technique

Poly[2-methoxy-5-(2'-ethylhexyloxy)-1,4-(1-cyanovinylene) phenylene] (MEH-CN-PPV) and poly[2-methoxy-5-(2'-ethylhexyloxy)-1,4-phenylene vinylene] (MEH-PPV), which are electron- and hole-transporting conjugated polymers, respectively, are of particular interest as organic matrices in organic/inorganic hybrid nanocomposite multi-spectral IR photodetectors deposited on GaAs substrates. Typically, such conjugated polymers are solution cast into thin films for device fabrication using techniques such as drop-casting, Langmuir Blodgett deposition, ink-jet printing, spraying, and spin-casting. However, depending on the solvent or deposition process used, individual polymer chains can become bent or wrapped around themselves on the substrate surface. Such conformational defects can strongly influence the optoelectronic behavior of conjugated polymers due to intrachain or interchain effects.

Matrix assisted pulsed laser evaporation (MAPLE) uses an IR laser wavelength tuned to a specific bond stretch or bond bend vibrational absorption peak in the host matrix of the target in order to reduce polymer damage. MEH-CN-PPV and MEH-PPV both lack a hydroxyl bond stretch, so MAPLE deposition using a laser at 2.9 μm can target hydroxyl bonds in the matrix. An important contribution of this work is the development of an emulsion technique to tune to number of hydroxyl bonds in the MAPLE target. In this way, excellent thin film deposition for both MEH-CN-PPV and MEH-PPV has been achieved. MAPLE deposition of MEH-PPV using the emulsion target yields films superior to those achieved by drop-casting with nearly

featureless surface morphology, and an impressive RMS surface roughness of 0.292 nm, as shown in the optical micrographs of Fig. 8. The MAPLE of light emitting conjugated polymer ultra-smooth thin films has important implications for realizing organic semiconductor photonic devices, as well as novel multi-layer organic device architectures.

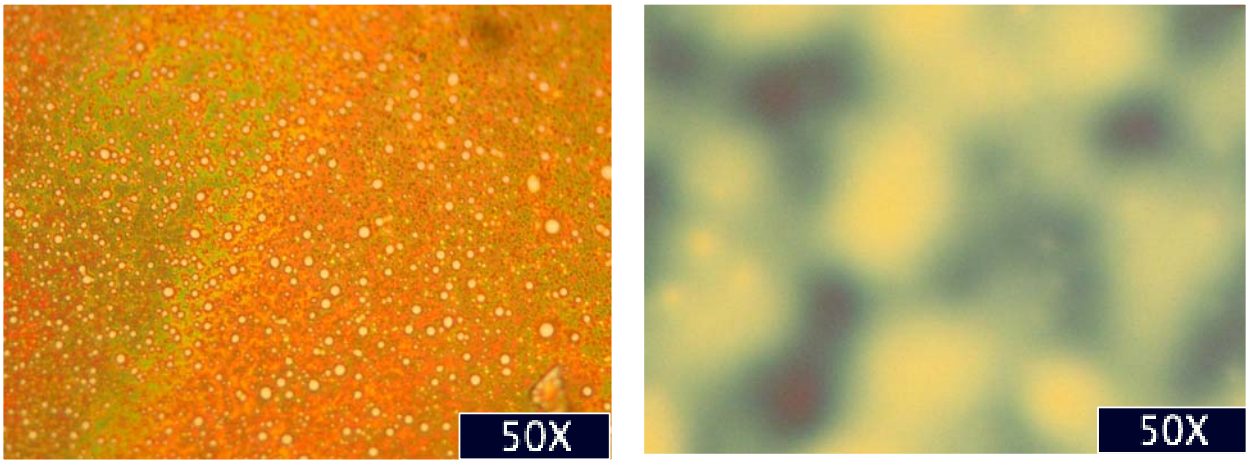

(a) (b)

Figure 8. Microscope images of (a) drop-cast MEH-PPV film characterized by a pitted texture due to solvent evaporation post- deposition, and (b) MAPLE-deposited MEH-PPV film demonstrating smooth, featureless surface.

Integration of InAs/GaAs EQDs with Two-Dimensional Photonic Crystal Cavities and PbS CQDs with One-Dimensional Photonic Crystal Cavities for Enhanced Absorption and Spectral Selectivity

A major goal of this program was to demonstrate enhanced absorption and spectral selectivity by integrating EQDs and CQDs in PC cavities. These goals were achieved by i) embedding InAs/GaAs EQDs in a 2D PC cavity fabricated by etching an array of air holes in the EQD active region; and ii) embedding PbS CQDs in a 1D PC cavity by depositing distributed Bragg reflectors (DBRs) of polymers.

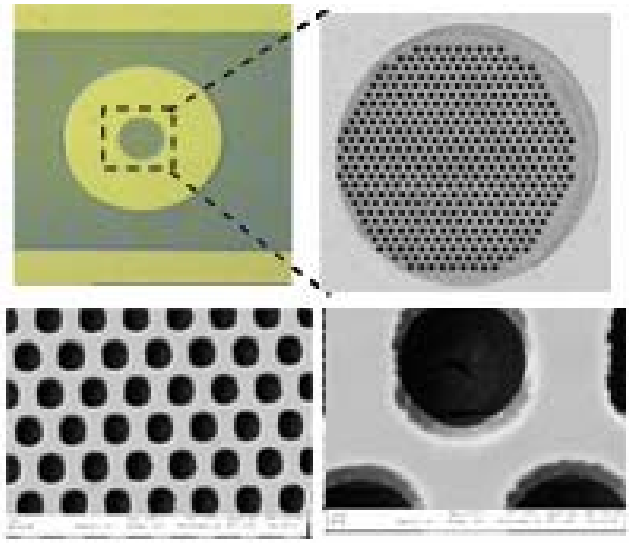

Figure 9. SEM top view images of fabricated device with defect-free PC cavity.

Fig. 9 shows SEM images of the fabricated device top view for a 2D PC in an InAs/GaAs EQD IR photodetector. Reference devices without 2D PC cavities were also fabricated for comparison. The variable-temperature IR spectral response shown in Figs. 10(a-c) demonstrates a two-fold increase in responsivity with the incorporation of the PC cavity at 55K. In addition, reference devices without PCs demonstrate a spectral response up to 57K, while those with PCs demonstrate a spectral response up to 91K. Thus, enhanced IR absorption is demonstrated in IR photodetectors incorporating 2D PC cavities with InAs/GaAs QDs. However, a distinct

enhancement in a specific defect mode location is not observed, which may be due to the relative low Q and relaxed absorption momentum selection rule. Based on the modeling, high spectral selectivity is achievable only with the optimization in coupled defect cavity design.

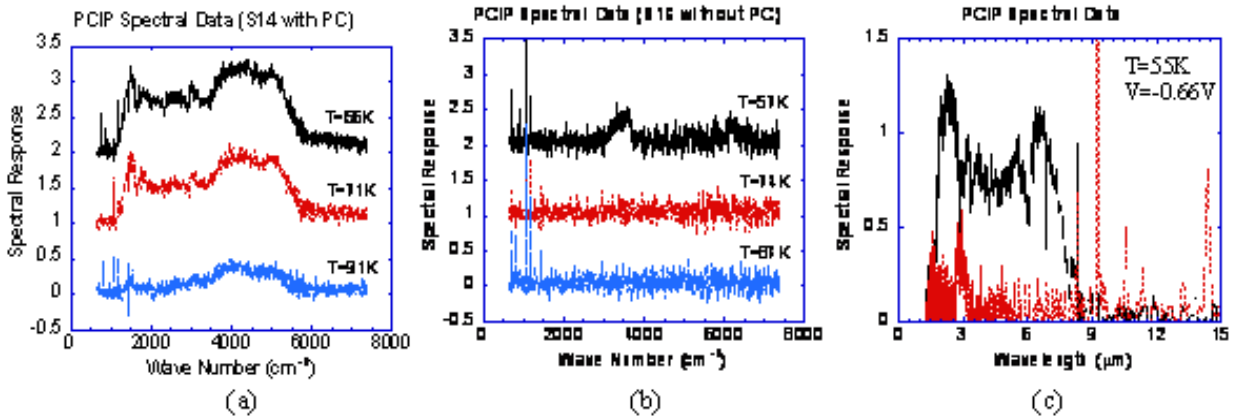

Figure 10. Measured spectral responses (a) with and (b) without photonic crystal cavities; (c) enhanced spectral response with the incorporation of photonic crystal cavities.

A second attempt to integrate a 2D PC cavity with an InAs/GaAs EQD IR photodetector was successful in enhancing a specific defect mode. The variable temperature IR spectral response, measured using FTIR spectroscopy, is shown for the InAs/GaAs QD IR photodetector and reference device without a PC cavity in Figs. 11(a) and (b), respectively. In general, the spectra for both devices are very similar at each temperature. However, it is important to note the spectra at 17 K in the range of 1000-2000 wavenumbers (or 5-10 μm). A distinct enhancement in the peak just below 1500 wavenumbers is observed in the device with a photonic crystal cavity. This peak corresponds to approximately 8 μm, which is the designed defect mode of the cavity. This is a significant advancement from earlier attempts that did not demonstrate enhancement of the

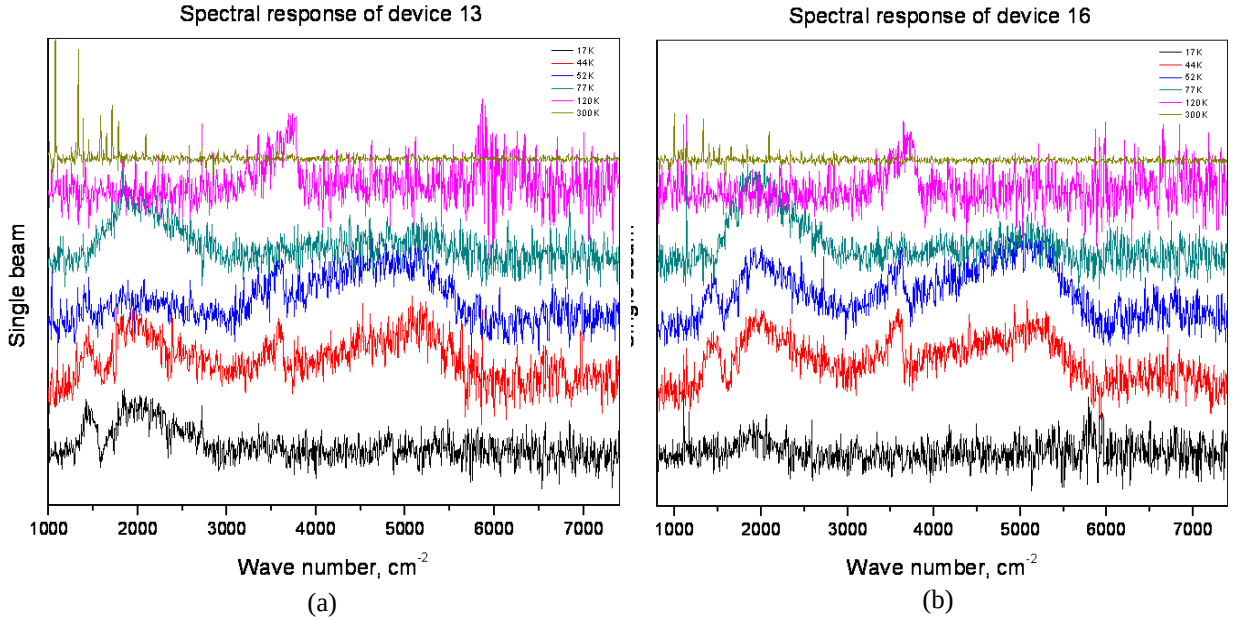

Figure 11. Spectral response measurements on InAs/GaAs QDIPs (a) with and (b) without photonic crystal cavities.

designed defect mode. However, this enhancement was observed only for very low temperatures. These results directed research towards a new approach described in the final section that uses Fano resonances in PCs.

The MAPLE growth techniques developed in this project enabled the novel demonstration of a 1D PC cavity appropriate for CQDs by depositing organic polymer DBRs. These structures require very careful control over film thickness and surface roughness, and the emulsion technique developed in this work was integral to the deposition of the required high quality organic films. The 1D PCs, based on repeated layers of PMMA and P3HT, were used to enhance near-IR absorption in PbS CQDs. Thin films of PMMA and P3HT were deposited by MAPLE. The film thickness was measured using atomic force microscopy, and the film refractive index was measured using spectroscopic ellipsometry. For PMMA, the film thickness was 189.2 nm and the refractive index was 1.4893. For P3HT, the film thickness was 140.9 nm and the refractive index was 2.0. These values were used to calculate the reflectivity for a DBR comprising 2, 4, 6, and 8 periods of the two layers designed to peak at 1.127 μm, as shown in Fig. 12 (a). A 4-period, PMMA/P3HT DBR was deposited by MAPLE, using the same film thicknesses, and the reflectivity was also measured, as shown in Fig. 12 (b). For the measured DBR, the peak reflectivity occurred at approximately 4.7 μm. This significant offset in wavelength is most likely due to an error in the refractive index measurement. However, as demonstrated by the clearly visible reflectivity peaks, the thin film thicknesses were well controlled by the MAPLE deposition. In order to demonstrate the enhanced absorption and spectral selectivity possible by embedded CQDs in a 1D PC cavity, the peak indicated at 2.4 μm was chosen for a complete cavity demonstration. This wavelength was chosen due to the availability of PbS CQDs (diameter = 12.9 nm) with bandgaps corresponding to this value.

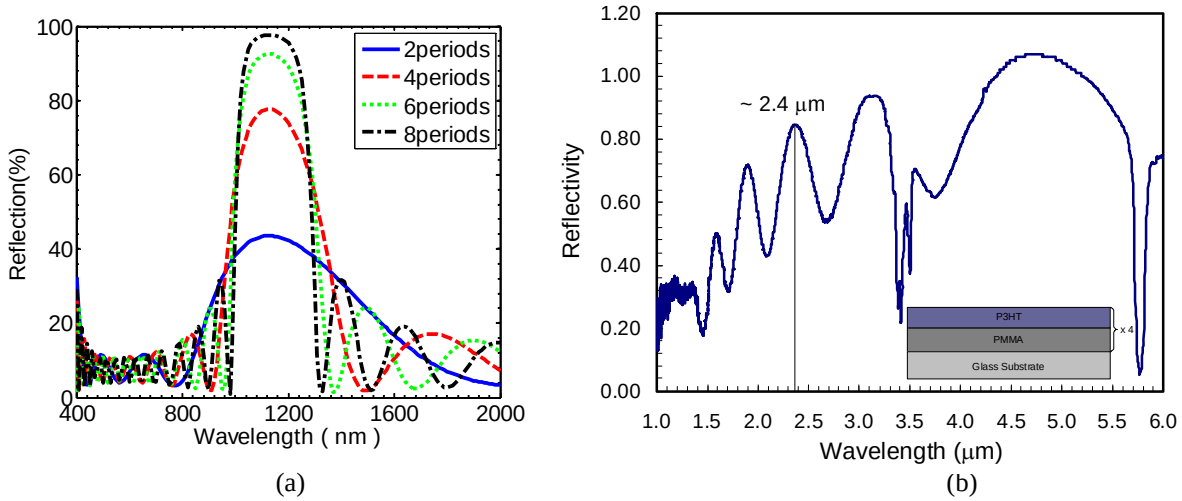

Figure 12. (a) Calculated reflectivity for PMMA/P3HT DBRs at 1.127 μm using measured film thicknesses and refractive indices after thin-film MAPLE deposition; and (b) measured reflectivity for a 4 period PMMA/P3HT DBR.

As shown in Fig. 13, PbS CQDs were embedded in a full 1D PC cavity comprising PMMA/P3HT DBRs on either side of the CQD active region. Fig. 13(a) shows a schematic diagram of the structure. FTIR absorbance measurements were conducted for the PbS CQDs alone and embedded in the PC cavity, as shown in Fig. 13(b). At the relevant wavelength near 2.4 μm, the 1D PC cavity contributed to an absorption enhancement of 10-20. This is a

substantial increase in absorption at the desired wavelength and is an important demonstration of the value of this approach to achieving multi-spectral photodetection using CQDs.

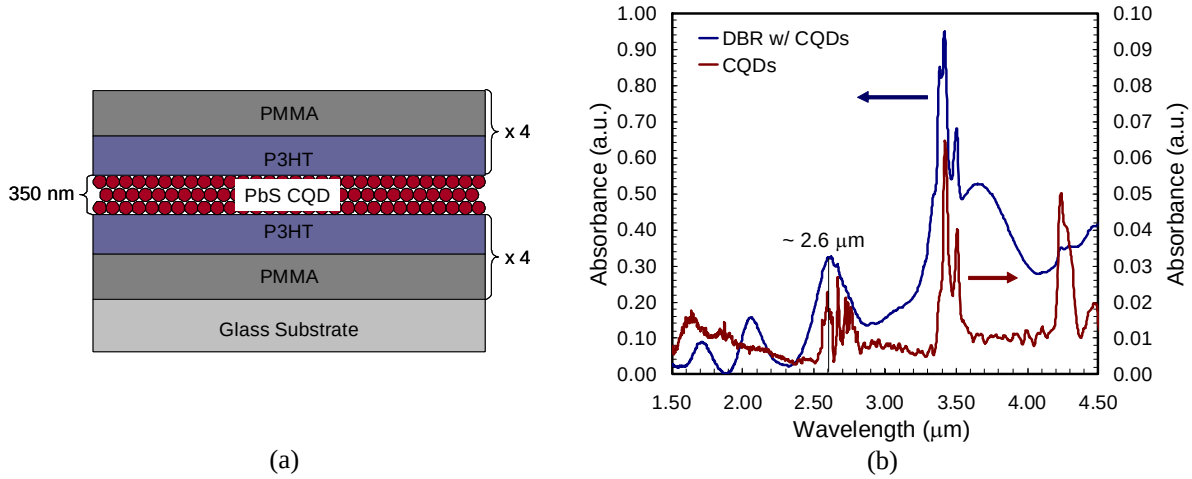

(a) (b)

Figure 13. (a) Schematic diagram of PbS CQDs embedded in a 1D PC cavity comprising DBRs of PMMA/P3HT; and (b) the measured FTIR absorbance of the CQDs and the CQDs embedded in the cavity, demonstrating an enhancement of 10-20.

Tuning Fano Resonance Filters by Integration of CQDs for Enhanced Absorption and Spectral Selectivity

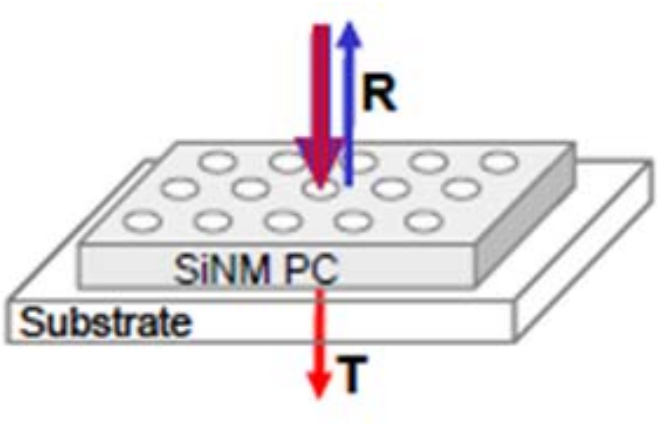

Figure 14. Schematic diagram of Fano filter comprising silicon nanomembrane mounted on a glass substrate.

A final important contribution of this work is the demonstration of a new type of spectrally selective photodetector based on Fano resonances in periodic structures and stacked nanomembranes on glass and flexible substrates, as shown schematically in Fig. 14. Compared to traditional PC cavities that use defects in the bandgap regime, Fano resonances use guided modes and are defect free. This is an important advantage as it has been difficult to match the designed PC cavity defect mode with the absorption peak of a given InAs/GaAs QD ensemble. Initial theoretical studies have demonstrated enhanced IR absorption of at least two orders of magnitude due to Fano resonances in PCs. Near-IR Fano resonance-based surface normal filters have been demonstrated experimentally, as well, based on patterned silicon nanomembranes transferred onto glass and flexible substrates.

Another important advantage of the Fano resonance approach is that spectral, angular, and polarization properties can be designed and controlled, leading to multi-parametric IR absorption and detection. A refractive index change of the filter depends upon the incidence angle and light polarization, and can cause a spectral shift or change in intensity of the IR absorption spectrum,

enabling the measurement of spectral, angular, and polarization properties. A unique approach to controlling these properties is to fill the air holes of a Fano filter with PbS CQDs (with or without an organic matrix). MAPLE deposition was used to fill air holes in 2D photonic crystal Fano resonance filters on silicon nanomembranes with PbS CQDs, as shown in Fig. 15. These SEM images show the bare Fano filter nanomembrane (Fig. 15(a)), the nanomembrane after MAPLE deposition (Fig. 15(b)), and the nanomembrane after cleaning the surface to reveal the PbS CQDs within the air holes (Fig. 15(c)). Preliminary results indicate that MAPLE deposition achieved a better fill factor of the air holes than other techniques of CQD deposition.

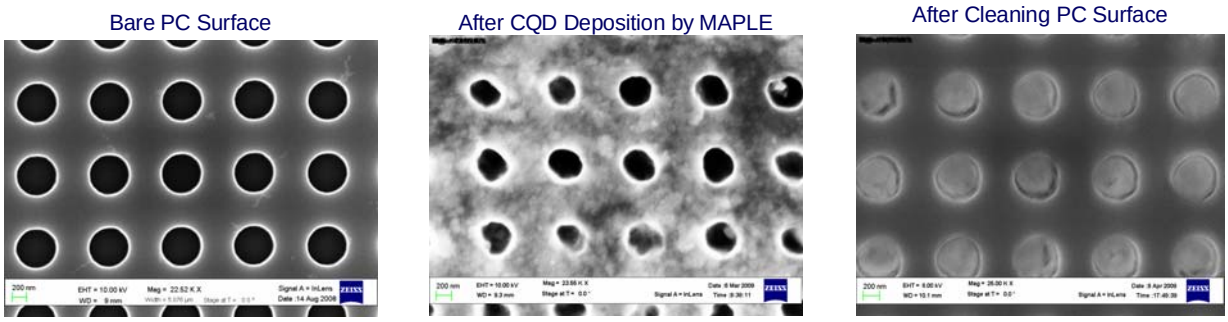

(a) (b) (c)

Figure 15. SEM images of Fano filter air holes (a) before and (b) after MAPLE deposition of PbSe CQDs and (c) after cleaning surface.

Fig. 16 shows reflection and absorption measurements of the Fano filter with and without filling the air holes with MAPLE-deposited PbS CQDs. By comparing both, it is observed that filling the air holes induces a large reflection and absorption change at the Fano spectral resonance. Thus, this work has demonstrated an important new technique to achieve more control over IR absorption by combining CQDs with PC cavities.

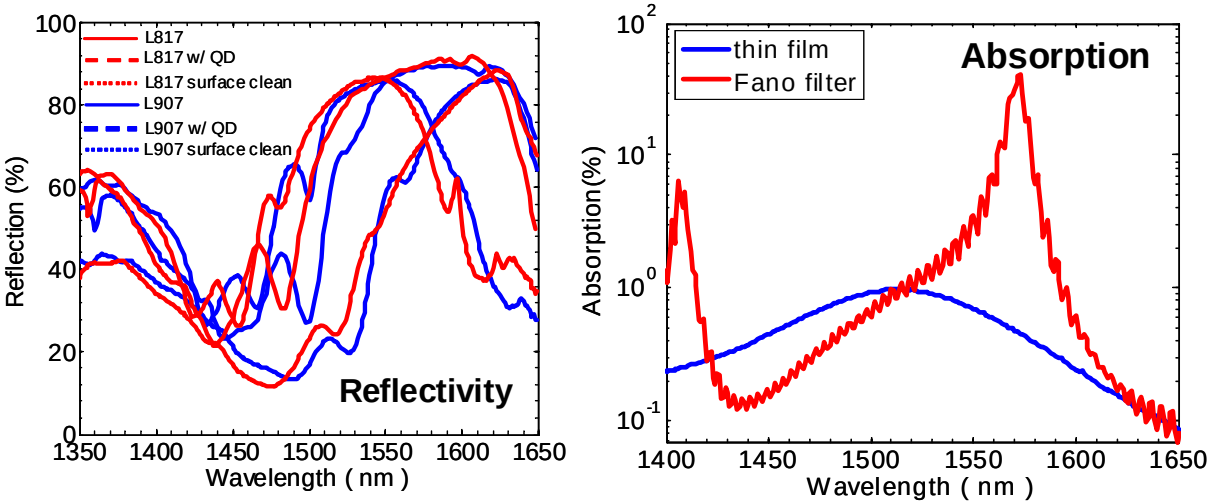

(a) (b)

Figure 16. (a) Measured reflectivity for two different samples before and after MAPLE deposition (both w CQDs on the surface and after the surface was cleaned); and (b) measured absorption for the PbS CQD thin film and the Fano filter with PbS CQDs demonstrating enhanced absorption.

Archival Publications Resulting from Grant

Archival Journal Articles

1. L. Chen, H. Yang, Z. Qiang, H. Pang, L. Sun, Z. Ma, R. Pate, **A. Stiff-Roberts**, S. Gao, J. Xu, **G. J. Brown**, and **W. Zhou**, "Colloidal quantum dot absorption enhancement in flexible Fano filters," *Applied Physics Letters*, vol. 96, pp. 083111, February 2010.
2. **A. D. Stiff-Roberts**, K. R. Lantz, and R. Pate, "Room-temperature, mid-infrared photodetection in colloidal quantum dot/conjugated polymer hybrid nanocomposites: a new approach to quantum dot infrared photodetectors," *Journal of Physics D: Applied Physics*, vol. 42, pp. 234004, November 2009.
3. **A. D. Stiff-Roberts**, "Quantum Dot Infrared Photodetectors: Advantages, Challenges, and Future Research Directions," (INVITED), *Proceedings of the 9th Annual IEEE Conference on Nanotechnology (IEEE NANO 2009)*, pp. 537-542, July 2009.
4. L. Chen, Z. Qiang, H. Yang, H. Pang, Z. Ma, and **W. D. Zhou**, "Polarization and angular dependent transmissions on transferred nanomembrane Fano filters," *Optics Express*, vol. 17, p.8396, May 2009.
5. **A. D. Stiff-Roberts**, "Quantum Dot Infrared Photodetectors: A Review," (INVITED) *Journal of Nanophotonics*, vol. 3, p. 031607, April 2009.
6. L. Chen, H. Yang, Z. Qiang, H. Pang, Z. Ma, J. Xu, **G. J. Brown**, and **W. D. Zhou,** "Angle and Polarization Dependent Characteristics of Colloidal Quantum Dot Absorption in Fano Filters on Flexible Substrates", *Proceedings of the SPIE*, vol. 7222, p. 72220V, January 2009.
7. Z. Qiang, L. Chen, H. Yang, H. Pang, Z. Ma, and **W. D. Zhou**, "Fano filter modal analysis based on transferred silicon nanomembranes on flexible substrates", *Applied Physics Letters*, vol. 93, p. 061106, August 2008.
8. Z. Qiang, L. Chen, H. Yang, H. Pang, Z. Ma, and **W. D. Zhou**, "Fano filter modal analysis based on transferred silicon nanomembranes on flexible substrates", *Proceedings of the SPIE*, vol. 7031, p. 703109, August 2008.
9. R. Pate, K. R. Lantz, and **A. D. Stiff-Roberts**, "Tabletop resonant infrared matrix-assisted pulsed laser evaporation of light-emitting organic thin films," *IEEE Journal of Selected Topics in Quantum Electronics (Semiconductor Photonic Materials)*, vol. 14 , p. 1022, July/August 2008.
10. H. Yang, Z. Qiang, H. Pang, Z. Ma, and **W. D. Zhou**, "Surface-normal Fano filters based on transferred silicon nanomembranes on glass substrates", *Electronics Letters*, vol. 44, p. 858, July 2008.
11. **A. D. Stiff-Roberts** and K. R. Lantz, "Room-temperature, Intraband, Infrared Absorption in CdSe/MEH-PPV Nanocomposites Drop-Cast on GaAs," *Journal of Applied Physics*, vol. 103, pp. 104316, June 2008. Also appeared at *Virtual Journal of Nanoscale Science & Technology*, vol. 17 (23), June 2008.
12. Z. Y. Zhao, W. M. Zhang, C. Yi, **A. D. Stiff-Roberts**, B. J. Rodriguez, and A. P. Baddorf, "Doping Characterization of InAs/GaAs Quantum Dot Heterostructure by Cross-Sectional Scanning Capacitance Microscopy," *Applied Physics Letters*, vol. 92, pp. 092101, March 2008. Also appeared at *Virtual Journal of Nanoscale Science & Technology*, vol. 17 (11), March 2008.
13. Z. Qiang, **W. D. Zhou**, M. Lu, and **G. J. Brown**, "Fano resonance enhanced infrared absorption for infrared photodetectors", *Proceedings of the SPIE*, vol. 6901, p. 69010F, January 2008.

14. Z. Y. Zhao, C. Yi, **A. D. Stiff-Roberts**, A. J. Hoffman, D. Wasserman, and C. Gmachl, "Probing Dopant Incorporation in InAs/GaAs QDIPs by Polarization-Dependent Fourier Transform Infrared Spectroscopy," *Infrared Physics & Technology*, vol. 51, pp. 131-135, October 2007.
15. R. A. Soref, Z. Qiang, **W. D. Zhou**, "Far infrared photonic crystals operating in the Reststrahl region", *Optics Express*, vol. 15, pp. 10637-48, August 2007.
16. Z. Zhao, C. Yi, K. R. Lantz, and **A. D. Stiff-Roberts**, "Effect of donor-complex-defect-induced dipole field on InAs/GaAs quantum dot infrared photodetector activation energy," *Applied Physics Letters*, vol. 90, pp. 233511-1-3, June 2007. Also appeared in *Virtual Journal of Nanoscale Science & Technology*, vol.15 (24), 2007.
17. **W. D. Zhou**, L. Chen, Z. Qiang, and **G. J. Brown**, "Spectrally selective infrared absorption in defect-mode photonic-crystal-slab cavity," *Journal of Nanophotonics*, vol. 1, paper 013515, June 2007.
18. Z. Zhao, C. Yi, **A. D. Stiff-Roberts**, A. J. Hoffman, D. Wasserman, and C. Gmachl, "DX-like centers in InAs/GaAs QDIPs observed by polarization-dependent Fourier transform infrared spectroscopy," *Journal of Vacuum Science and Technology B*, vol. 25, pp. 1108-1112, May/Jun 2007.
19. **W. D. Zhou**, Z. X. Qiang, and L. Chen, "Photonic crystal defect mode cavity modeling: a phenomenological dimensional reduction approach," (INVITED) *Journal of Physics D: Applied Physics*, vol. 40, pp. 2615-2623, May 2007 (Special issue on photonic crystal devices).
20. **A. D. Stiff-Roberts**, "Hybrid Nanomaterials for Multi-spectral Infrared Photodetection," *International Journal of High Speed Electronics and Systems*, vol. 17, pp. 165-172, March 2007.
21. Z. X. Qiang and **W. D. Zhou**, "Effective index perturbation: Correlations between the photonic bandgap and the donor-like defect mode in photonic crystal slabs," *Proceedings of the SPIE*, vol. 6468, paper 64680M, March 2007.
22. Z. Qiang, **W. Zhou**, and R. A. Soref, "Optical add-drop filters based on photonic crystal ring resonators," *Optics Express*, vol. 15, pp. 1823-1831, February 2007. Also appeared in *Virtual Journal of Nanoscale Science & Technology*, vol.15 (9), 2007.
23. L. Chen, Z. X. Qiang, **W. D. Zhou**, and **G. J. Brown**, "Spectral selective absorption enhancement in photonic crystal defect cavities," *Proceedings of the SPIE*, vol. 6480, paper 64801C, February 2007.
24. E. B. Stokes, **A. D. Stiff-Roberts**, and C. T. Dameron, "Quantum dots in semiconductor optoelectronic devices," *The Electrochemical Society Interface*, Winter, pp. 23-27, 2006.
25. L. Chen, **W.D. Zhou**, Z. X. Qiang, and **G. Brown**, "Spectral selectivity of photonic crystal infrared photodetectors," *Proceedings of the SPIE*, vol. 6370, paper 63701I, October 2006.
26. Z. Qiang and **W. D. Zhou**, "Fast calculation of cavity-mode characteristics of photonic crystal cavities," *IEEE Photonics Technology Letters*, vol. 18, pp.1940-1942, September 2006.

Archival Conference Proceedings

27. R. Pate, K. R. Lantz, A. Dhawan, T. Vo-Dinh, and **A. D. Stiff-Roberts**, "Resonant infrared matrix-assisted pulsed laser evaporation of inorganic nanoparticles and organic/inorganic hybrid nanocomposites," *International High-Power Laser Ablation Conference*, Santa Fe, NM, April 2010.

28. L. Chen, H. Yang, Z. Qiang, L. Sun, Z. Ma, R. Pate, **A. Stiff-Roberts**, J. Xu, **G. J. Brown**, and **W. Zhou**, "Direct measurement of spectrally selective absorption enhancement in Fano resonance photonic crystal cavities on plastic substrates," *SPIE Photonics West*, San Francisco, CA, January 2010.
29. **A. D. Stiff-Roberts**, "Quantum Dot Infrared Photodetectors: Advantages, Challenges, and Future Research Directions," (INVITED) *9th Annual IEEE Conference on Nanotechnology (IEEE NANO 2009)*, Genoa, Italy, July 2009.
30. **A. D. Stiff-Roberts**, "Hybrid Nanomaterials for Multi-spectral Infrared Photodetection," (INVITED), *2009 Nanotechnology for Defense Conference*, Burlingame, CA, April 2009.
31. Y. Wang, L. Chen, H. Yang, Q. Guo, **W. D. Zhou**, and M. Tao, "Anti-Reflection and High-Reflection Optical Thin Films Based on Dip Coating of Inorganic Particles", *Materials Research Society Fall Meeting*, Boston, MA, December 2008.
32. **W. D. Zhou**, "Heterogeneous Material Integration with Photonic Crystal Platforms for Nanophotonic Devices on Silicon", (INVITED) *27th International Congress on Applications of Lasers & Electro-Optics*, Temecula, CA, October 2008.
33. **A. D. Stiff-Roberts**, "Photonic Nanomaterials for Infrared Photodetection," (INVITED), *The 8th Annual Meeting of the Fitzpatrick Institute for Photonics*, Durham, NC, October 2008.
34. Z. Qiang, H. Yang, L. Chen, H. Pang, Z. Ma, **W. D. Zhou,** and **G. J. Brown**, "Characteristics of Surface-Normal Fano Filters on Plastic Substrates", *IEEE International Conference on Nanotechnology*, Arlington, TX, August 2008.
35. **W. D. Zhou**, H. Yang, Z. Qiang, L. Chen, and **G. J. Brown**, "Spectrally Selective Infrared Absorption Enhancement in Photonic Crystal Cavities," (INVITED) *SPIE Annual Meeting*, San Diego, CA, August 2008.
36. H. Yang, Z. Qiang, H. Pang, Z. Ma, **W. D. Zhou**, M. Lu, and R. A. Soref, "Surface-Normal Fano Filters Based on Transferred Silicon Nanomembranes on Glass Substrates", *Conference on Lasers and Electro Optics*, San Jose, CA, May 2008
37. Z. Qiang, **W. D. Zhou**, M. Lu, and G**. J. Brown**, "Fano Resonance Enhanced Infrared Absorption for Infrared Photodetectors", *Photonics West*, San Jose, CA, January 2008
38. H. Yang, L. Chen, Z. Qiang, **W. D. Zhou**, W. Zhang, **A. D. Stiff-Roberts**, S. Krishna, and **G. J. Brown**, "Characteristics of photonic crystal cavity based infrared photodetectors," *Lasers and Electro-Optics Society Meeting*, Lake Buena Vista, FL, October 2007.
39. Z. Y. Zhao, W. M. Zhang, C. Yi, **A. D. Stiff-Roberts**, B. J. Rodriguez, and A. P. Baddorf, "Doping characterization on InAs/GaAs quantum dot heterostructure by cross-sectional scanning capacitance microscopy," *Lasers and Electro-Optics Society Meeting*, Lake Buena Vista, FL, October 2007.
40. **W. D. Zhou**, H. Yang, L. Chen, Z. Qiang, **A. D. Stiff-Roberts**, and **G. J. Brown**, "Photonic crystals for spectrally selective infrared photonics," (INVITED) *The 6th Asia-Pacific Conference on Near-Field Optics*, Yellow Mountain, China, June 2007.
41. R. Pate, K. Lantz, and **A. Stiff-Roberts**, "Matrix-assisted pulsed laser evaporation of hybrid colloidal quantum dot/conducting polymer nanocomposite heterostructures," *Electronic Materials Conference*, Notre Dame, IN, June 2007.
42. Z. Zhao, K. R. Lantz, C. Yi, and **A. D. Stiff-Roberts**, "Doping effect on carrier occupation and transport in InAs/GaAs quantum dot infrared photodetectors: A capacitance-voltage spectroscopy study," *Conference on Lasers and Electro-Optics*, Baltimore, MD, May 2007 (poster).

43. Z. X. Qiang and **W. D. Zhou**, “Effective index perturbation: Correlations between the photonic bandgap and the donor-like defect mode in photonic crystal slabs,” *Photonics West*, San Jose, CA, January 2007.
44. L. Chen, Z. X. Qiang, **W. D. Zhou**, and **G. J. Brown**“ Spectrally selective absorption enhancement in photonic crystal defect cavities,” *Photonics West*, San Jose, CA, January 2007.
45. Z. Zhao, C. Yi, **A. D. Stiff-Roberts**, A. J. Hoffman, D. Wasserman, and C. Gmachl, “DX centers in InAs/GaAs QDIPs observed by polarization-dependent Fourier transform infrared spectroscopy,” *North American Conference on Molecular Beam Epitaxy*, Durham, NC, October 2006 (poster)
46. **A. D. Stiff-Roberts**, “Hybrid nanomaterials for multi-spectral infrared photodetection,” (INVITED) *Lester Eastman Conference on High Performance Devices*, Ithaca, NY, August 2006.